Elsevier Editorial System(tm) for Chemical Geology
Manuscript Draft

Manuscript Number:

Title: Gas blowout from shallow boreholes near Fiumicino International Airport (Rome): gas origin and hazard assessment

Article Type: Research Article

Keywords: Endogenous gas blowout from shallow wells, Chemical and isotopic composition of gas and water, Viscous flux and diffuse soil gas flux measurements, Simulation and monitoring of air CO_2 dispersion, Hazard assessment

Corresponding Author: Dr. Maria Luisa Carapezza,

Corresponding Author's Institution: Istituto Nazionale Geofisica e Vulcanologia

First Author: Maria Luisa Carapezza

Order of Authors: Maria Luisa Carapezza; luca tarchini, researcher; domenico granieri, senior technologist; mauro martelli, researcher; Alessandro Gattuso , researcher; Nicola M Pagliuca , researcher; Massimo Ranaldi , researcher; Tullio Ricci , researcher; Fausto Grassa , researcher; Andrea Rizzo, researcher; Luca Pizzino , researcher; Alessandra Sciarra , researcher

Abstract: In summer 2013 a toxic and polluting gas blowout (19 ton day^{-1} CO_2, 95 kg day^{-1} CH_4) occurred from two shallow boreholes drilled at only 50 m from the International Airport of Rome (Italy), in the town of Fiumicino. Another gas blowout occurred in the same period from a borehole located offshore, 2 km away, also generating sea-water acidification; it lasted only a couple of days. Onshore, CO_2 was also diffusing from holes within the soil, particularly towards the airport, generating a soil flux up to 1.8 ton day^{-1}. In 3.5 months ~1500 tons of CO_2 and 5.4 tons of CH_4 were emitted in the atmosphere. Temporal monitoring of gas geochemistry indicates that in this area a mixing occurs between shallow and pressurized gas pockets, CO_2-dominated, but with different chemical (i.e., He/CH_4 ratio) and isotopic ($^3He/^4He$, □13C-□DCH4) characteristics. Numerical simulation of CO_2 dispersion in the atmosphere showed that dangerous air CO_2 concentrations, up to lethal values, were only found near the vents at a height of 0.2 m. Fiumicino is a high blowout risk area, as CO_2 rising through deep reaching faults pressurizes the shallow aquifer confined underneath shales of the Tiber delta deposits. The Fiumicino blowout is a typical example of dangerous phenomenon that may occur in urban context lying nearby active or recent volcanoes and requires quick response on hazard assessment by scientists to be addressed to civil protection and administrators.

Highlights

Gas and mud emission occurred in 2013 from shallow boreholes close by Rome Airport.

Gas consisted of a mixture of CO_2 and CH_4 rising through deep reaching faults.

Isotope geochemistry suggest a deep mantle or magmatic origin for CO_2.

Chemistry of muddy water confirms seawater intrusion in pressurized onshore aquifer.

Gas hazard assessed by monitoring air [CO_2] and simulating air dispersion.

Gas blowout from shallow boreholes near Fiumicino International Airport (Rome): gas origin and hazard assessment

Maria Luisa Carapezza [1,*], Luca Tarchini [2], Domenico Granieri [3], Mauro Martelli [4], Alessandro Gattuso [1], Nicola Pagliuca [1], Massimo Ranaldi [2], Tullio Ricci [1], Fausto Grassa [4], Andrea Rizzo[4], Luca Pizzino [1], Alessandra Sciarra [1]

[1]Istituto Nazionale di Geofisica e Vulcanologia, Sez. Roma 1, Via di Vigna Murata 605, 00143 Roma, Italy.
[2]Dipartimento di Scienze, Università di Roma Tre, Largo S. Leonardo Murialdo 1, 00146 Roma, Italy.
[3]Istituto Nazionale di Geofisica e Vulcanologia, Sez. Pisa, Via della Faggiola, 32, 56126 Pisa, Italy.
[4]Istituto Nazionale di Geofisica e Vulcanologia, Sez. Palermo, Via Ugo La Malfa, 153, 90146 Palermo, Italy.

[*]*Corresponding author: Maria Luisa Carapezza, Istituto Nazionale di Geofisica e Vulcanologia, Sez. Roma 1, via Vigna Murata, 605, 00143 Roma, Italy. E-mail: marialuisa.carapezza@ingv.it. Tel.: +390651860370.*

Abstract

In summer 2013 a toxic and polluting gas blowout (19 ton day^{-1} CO_2, 95 kg day^{-1} CH_4) occurred from two shallow boreholes drilled at only 50 m from the International Airport of Rome (Italy), in the town of Fiumicino. Another gas blowout occurred in the same period from a borehole located offshore, 2 km away, also generating sea-water acidification; it lasted only a couple of days. Onshore, CO_2 was also diffusing from holes within the soil, particularly towards the airport, generating a soil flux up to 1.8 ton day^{-1}. In 3.5 months ~1500 tons of CO_2 and 5.4 tons of CH_4 were emitted in the atmosphere. Temporal monitoring of gas geochemistry indicates that in this area a mixing occurs between shallow and pressurized gas pockets, CO_2-dominated, but with different chemical (i.e., He/CH_4 ratio) and isotopic ($^3He/^4He$, $\delta^{13}C$-δD_{CH4}) characteristics. Numerical simulation of CO_2 dispersion in the atmosphere showed that dangerous air CO_2 concentrations, up to lethal values, were only found near the vents at a height of 0.2 m. Fiumicino is a high blowout risk area, as CO_2 rising through deep reaching faults pressurizes the shallow

aquifer confined underneath shales of the Tiber delta deposits. The Fiumicino blowout is a typical example of dangerous phenomenon that may occur in urban context lying nearby active or recent volcanoes and requires quick response on hazard assessment by scientists to be addressed to civil protection and administrators.

Key Words: Endogenous gas blowout from shallow wells, Chemical and isotopic composition of gas and water, Viscous flux and diffuse soil gas flux measurements, Simulation and monitoring of air CO_2 dispersion, Hazard assessment.

1. Introduction

Rome city is located between two Quaternary volcanoes, Albani Hills and Mts. Sabatini, belonging to the alkali potassic Roman comagmatic Province (Fig. 1). This zone of Central Italy, up to the Tyrrhenian seaside, is characterized by an anomalous release of endogenous gas (e.g. Tor Caldara, Lavinio, Ardea, Pomezia, Fiumicino, Palidoro in Fig. 1) mostly consisting of CO_2 (*Chiodini et al.,* 2004). Most of these emissions occur above structural highs (horsts) of buried Mesozoic carbonates that represent the main aquifer, often geothermal, of the area. Carbon dioxide, either generated by thermo-metamorphic reactions in the limestones and of deeper mantle or magmatic origin (*Minissale et al.,* 1997; *Chiodini et al.,* 2004 and references therein) accumulates at the top of the carbonatic horsts. From there it escapes to the surface along deep-reaching faults, generating moffettes and strong emissive areas where lethal accidents frequently befall people and animals (*Carapezza et al.,* 2003; *Carapezza and Tarchini,* 2007). Rising CO_2 partly dissolves in shallow aquifers, pressurizing them when they are confined underneath impervious layers. Dangerous blowouts have occurred, even in urbanized areas, when these pressurized aquifers have been reached by wells, at depths ranging from 350m to only 10-15m (*Carapezza et al.,* 2011; 2012 and references therein).

On 24 August and 6 September 2013, new gas blowouts occurred at Fiumicino (Rome) from two shallow boreholes drilled to a depth of 35 m and 40 m respectively, at an important traffic roundabout of the town (Coccia di Morto, hereafter CdM) (Fig. 2). In this town several similar accidents have occurred in recent years, as in 2005 (*Barberi et al.,* 2007 and Fig. 2) and the authorities were very concerned, both because of the emission of a toxic cloud in the urban area (nearest houses at only 100 m) and because a runway of fundamental importance for Fiumicino International Airport was only 50 m away (Fig. 2). We were therefore entrusted by regional Civil Protection to monitor the emission and assess the hazard. We periodically analyzed CdM gas and estimated the total gas output, until the emission was tentatively closed by borehole cementation on 18 December 2013; the water emitted by CdM vents was also sampled and diffuse CO_2 flux was repeatedly measured from the soil around the vents. Soil CO_2 flux was surveyed again on March and September 2014, in order to control the effectiveness of the remedies. Unfortunately, the latter survey showed the renewal of a significant soil CO_2 emission and even gas bubbling was visible above the badly cemented vents.

On 26 September 2013, another accidental gas blowout occurred offshore, just 400 m from the coast and 2.3 km WNW of CdM, creating new concern in the authorities and the population (Fig. 2 for location and Fig. 01 in Supplementary Material). This gas emission lasted only two days, due to the collapse of the vent walls. We measured gas concentration in air, the physico-chemical parameters of the seawater during and after the gas blowout and collected gas samples for chemical and isotopic analyses.

The onshore blowout episode has been already discussed in different studies; the characterization of CdM gas, collected in two days, and relation with tectonics are reported by *Ciotoli et al*. (2013); the geological and hydrological context of the area has been described by *Sella et al*. (2014) who, however, do not report any direct analytical data of the CdM gas emission. Finally, *Bigi et al.* (2014) drawn the tectonic setting of the Fiumicino area by means of a seismic reflection profile associated to soil gas surveys.

In this work we present new fundamental information, as data about the offshore gas emission (seafloor modification, seawater acidification, gas chemistry). We describe the scientific intervention carried out for monitoring the gas blowouts from their onset to the closure, along over three months of continuous emergency work with eleven sampling campaigns, the last one performed in September 2014 to verify the state of the site nine months after the hole cementation. The chemical and isotopic variations observed during monitoring are presented together with the results of the offshore gas chemical and isotopic analyses, necessary to understand the origin of the pressurized gas in the area. We estimated also the total amount of gas emitted by measurements of both the viscous flux from the boreholes and the diffuse flux through the soil. Finally, the CdM total gas flux and wind data have been used to simulate the gas dispersion in the atmosphere which has been compared with actual air gas concentration measurements in order to assess the related gas hazard.

2. Methods

2.1. Field measurements

To estimate the viscous gas flux, vent 1 was totally covered by a large plastic sheet laterally sealed to prevent air access (Fig. 02 in Supplementary Material), whereas the smaller vent 2 was covered by a large bucket. In both cases a tube of 15.5 cm diameter conveyed the gas outside and flow velocity was measured by a fan anemometer (Delta Ohm, AP472S1; range: 0.6-25m/s ±0.01m/s). From the same tube, gas samples for laboratory analyses were collected (Fig. 02 in Supplementary Material) and CO_2 and CH_4 fluxes were calculated from the concentration of the two gases. The offshore gas was sampled using a balloon, anchored to the sea bottom over the emission, and with an open bottom (50 cm across) and a tube at its top (Fig. 01 in Supplementary Material).

For air concentration measurements portable devices (Draeger X-AM 7000) equipped with IR detector for CO_2 (scale: 0-100 vol.%) and CH_4 (scale: 0-5 vol.%) were used. Continuous monitoring of air CO_2 concentration at CdM was carried out by three stations (see Fig. 2 for location), two of these devices equipped with IR spectrometers (Draeger, scale: 0-100 vol.%), were located in the proximity of the gas vents at 80 cm from the ground; data were acquired with a frequency of a minute. A third station (LI-IR detector, scale: 0-5 vol.%) was located 10 m far from the vents, at 30 cm high, and data acquisition had hourly frequency. This station was also equipped to continuously measure environmental parameters such as air and soil temperature (T), air and soil humidity (R.H.), atmospheric pressure (P), wind speed and direction (Fig. 03 in Supplementary Material).

Diffuse soil CO_2 flux was measured with the accumulation chamber method "time 0" (see *Chiodini et al.,* 1998 and *Carapezza and Granieri*, 2004 for description of the method); the device was equipped with a LI-820 infrared detector (scale: 0-2 vol.%, sensitivity: better than 0.1 g m^{-2} d^{-1}). The measurements were always carried out in dry and stable weather conditions to reduce a possible atmospheric influence on soil CO_2 flux.

Temperature, pH, redox potential (Eh), and electrical conductivity (salinity) of the water emitted were determined in the field with portable instruments previously calibrated with standard solutions. Alkalinity was measured through titration with 0.05 N HCl and methyl-orange as indicator. Physico-chemical parameters of seawater samples at the offshore emission were measured with the same portable instruments and seawater vertical profiles were acquired by a multi-parametric probe (Ocean Seven, Idronaut). Standard sensor specification of the probe are reported in Tab. 01 of Supplementary Material.

2.2. *Laboratory measurements*

Chemical and isotopic gas analyses were made at INGV-Palermo. Gas chemical composition and isotopic analyses of He, Ar and carbon of CO_2 were run accordingly with the procedures described by *Paonita et al*. (2012). Carbon and hydrogen isotopes of methane were carried out on a Delta Plus XP CF-IRMS instrument (Thermo, Bremen, Germany) coupled with a TRACE GC equipped with a Poraplot-Q capillary column (30 m x 0.32 mm i.d.) and using a flux of 0.8 cc min^{-1} of pure helium (5.6 grade) as gas carrier. GC III combustion interface was used to produce carbon dioxide from methane. GC-TC interface provides on-line high-temperature methane conversion into hydrogen suitable for isotope analyses. Typical reproducibility (1σ) for $\delta^{13}C_{CH4}$ and δD_{CH4} measurements is better than 0.2 ‰ and 2.5 ‰ respectively. Nitrogen isotope composition was determined using the procedure described by *Grassa et al*. (2010).

Water samples were filtered (through a 0.45 μm membrane) and stored in high-density polyethylene flacons. Major anions (Cl^-, Br^-, SO_4^{2-} and NO_3^-) and cations (Ca, Mg, Na and K) were analyzed by ion-chromatography (Dionex, DX500) on filtered and acidified samples, respectively. The analytical error for major elements was <10 %. The carbon isotopic ratio of TDIC, expressed as $\delta^{13}C$ ‰ vs. PDB, was analyzed by mass spectrometry (Finnigan Delta Plus) following the procedure described by *McCrea* (1950).

2.3. Geostatistical treatment of soil CO_2 flux data and modelling of gas dispersion in atmosphere

The normal probability plot of the soil CO_2 flux values measured on 26 August 2013 was used to establish the background threshold value (still in basically undisturbed conditions) and to identify anomalous populations (Fig. 3). The background is related to the so called "soil respiration", i.e. to a surficial emission of CO_2 of biological origin (*Parkinson*, 1981; *Reich et al.,* 2014). The background threshold has been estimated to 20 g m^{-2} d^{-1}, a value comparable with those of areas of Central Italy (background 10-25 g m^{-2} d^{-1}, *Carapezza and Tarchini*, 2007; *Carapezza et al*., 2012). The soil CO_2 flux maps were obtained using ordinary kriging in Golden Software Surfer®. Kriging allows to estimate the variable of interest at unsampled locations through a weighted linear combination of neighbouring observations over a regularly spaced grid. Soil CO_2 flux values were first log-transformed to obtain a normal distribution of the sample histogram. The specific semivariogram model for each survey was chosen as combinations of two survey-specific functions: a nugget effect accounting for short-scale variability, and an asymptotic function (spherical, rational quadratic or cubic) accounting for the statistical variability. The interpolation grid was then estimated on a 1×1 m spacing. Every estimated grid node was back-transformed in g m^{-2} d^{-1}, and multiplied by the node size (1 m^2): the anomalous CO_2 emission from the soil for each survey, together with its areal extent, could thus be calculated by summing the contribution of every grid node exceeding the background threshold.

The TWODEE-2 Eulerian code (*Folch et al*., 2009) was used to model the CO_2 dispersion in atmosphere. The code reproduces the dispersion of a gas cloud, denser than air, released from punctual and/or diffuse sources. Inputs to the model were topographic data (including terrain roughness), average winds on the computational domain and gas fluxes from the source(s). TWODEE-2 was coupled to the diagnostic wind model (DWM; *Douglas and Kessler,* 1990) in order to derive, from the wind measurements, a wind field that reproduces the effects of the morphology and soil-cover types within the scale of the domain. As result, TWODEE-2 yielded air CO_2 concentrations at selected heights.

3. **Description of events and viscous gas flux measurements**

3.3. *The 2013 Coccia di Morto blowouts*

The two onshore shallow boreholes that caused the gas emission were drilled at CdM at only 5 m from one another, to install conductive ground electrodes. The site is a traffic roundabout where a few meters of filling earth cover the Tiber delta sedimentary succession, made of fine sands, silts, shales and also containing levels of peat and peaty mud, typical of a fluvial and lagoon environment (*Milli et al*., 2013).

On 24 August 2013, a first vent emitting gas and mud opened and rapidly enlarged, taking on an elliptic shape of 2.5x1.6 m (Fig. 04 in Supplementary Material); it partly collapsed on 18 October and emission ended. The second CdM vent opened on 6 September and lasted until it was cemented over (Fig. 05 in Supplementary Material).

The viscous gas flux from vent 1 increased from 31 August (14.4 ton day $^{-1}$ of CO_2 and 47.85 kg day^{-1} of CH_4) to 6 September (18.7 ton day^{-1} of CO_2 and 59.84 kg day $^{-1}$ of CH_4). After the opening of vent 2, the flux from vent 1 decreased and the total gas output from the two vents was nearly the same as that previously recorded at vent 1 (17.65 ton day^{-1} of CO_2 and 57.18 kg day^{-1} of CH_4) (Fig. 4). After the collapse of vent 1 on 18 October, the gas output from vent 2 increased only slightly (from 6.35 to 8.0 ton day^{-1} of CO_2 and from 26 to 36.6 kg day^{-1} of CH_4) (Fig. 4).

3.4. The September 2013 offshore gas blowout

The offshore gas blowout (OS in Fig. 2) occurred on 26 September 2013, from a borehole only 5 cm in diameter drilled to -31m from the sea bottom (depth 7 m). On the morning of the following day, a degassing zone, a dozen of meters wide, with an intense bubbling activity generating small waves could be seen at the calm sea surface (Fig. 5). An anomalous content of CO_2 and CH_4 in air (20 vol.% and >5 vol.% respectively) was measured from a boat in the proximity of the gas emission. The gas could not be sampled because a strong centrifugal thrust did not permit the boat to approach the center of the degassing zone. Some seawater chemico-physical parameters were measured at the boundary of the emission zone, finding a low pH of 5.91 reflecting acidification by CO_2 dissolution (undisturbed seawater has pH ~8), a T of 23 °C and an electrical conductivity (Cond.) of 52.4 mS/cm. On 28 September, when gas was sampled, the emission was weaker and the gas was coming out as a myriad of small bubbles and microbubbles (Fig. 01 in Supplementary Materials). The seawater pH had slightly increased (pH= 6.70; T= 22.6 °C; Cond.= 55.3 mS/cm), remaining however still lower than in undisturbed seawater. A scan sonar survey and sub inspection revealed that a wide depression (diameter 6 m, depth 10 m) had formed in the seafloor, terminating in a conduit about 1 m large and extending down to 19 m (Fig. 6). On 2 October, when the gas emission was not anymore visible at the sea surface, a scan sonar and multiparametric probe survey showed that the depression on the sea bottom had almost disappeared (Figs. 6 and 7) and the seawater pH had returned to its normal value (8.2) (Figs. 7 and 8). The results of gas analysis are discussed in chapter *4.2*.

4. Water and gas geochemistry

4.1. Water chemistry

The muddy water emitted from vent 1 at CdM, sampled with a bucket in September 2013, had a temperature of 19°C, pH of 6.51, Eh of 105 mV, electrical conductivity of 39.7 mS/cm, TDS of 27,790 mg/l. Its chemical analysis (Table 1) indicates a chloride alkaline composition with high HCO_3^-, suggesting that it consisted mostly of CO_2-enriched seawater. Assuming that chloride is a conservative ion of marine origin and using the chloride mass balance through a mixing approach of seawater and fresh water (*Appelo and Postma*, 1994; *Terzić et al.,* 2010; *Trabelsi et al.,* 2012) it has been estimated that seawater represents 66 % of the CdM water. This confirms a well known phenomenon of the Fiumicino area, i.e. the seawater intrusion in the coastal aquifer mostly due to overpumping (*Capelli and Mazza*, 2008). The $\delta^{13}C_{CO2}$ (+3.20 ‰ vs. PDB) calculated from the isotopic analysis of TDIC is more positive than in the CdM gas phase (-1.8 to -1.2 ‰, Table 2). This suggests the occurrence of isotopic fractionation affecting TDIC due to the removal of the isotopically light carbon from the solution, as expected during a degassing process. Kinetic isotope fractionation of carbon between liquid and gaseous phases is particularly favoured when intense degassing and turbulence occur at surface, as observed at CdM vents.

4.2. Geochemical characteristics and origin of the emitted gases

The chemical and isotopic analyses of the 2013 onshore and offshore Fiumicino gas emissions are reported in Table 2. For the sake of comparison the analyses of the gas emitted in the 2005 blowout occurred nearby (Isola Sacra, IS in Fig. 2; *Barberi et al.,* 2007), together with the nearest most important natural manifestations (Palidoro and Canale Vignole; CV in Fig. 2) are also reported. The CdM gas consists mostly of CO_2 (97 vol.% on average) with minor N_2 (1.3-3.6 vol.%) and CH_4 (0.87-1.33 vol.%) and is similar to the 2005 IS blowout gas.

Helium isotopic composition of CdM varies in a narrow range ($^3He/^4He$ = 0.20-0.25 Ra). These values reflect a crustal-radiogenic source (i.e., 0.03 Ra; *O'Nions and Oxburgh*, 1988) mixed with a slightly variable amount of mantle He, which in the area has peculiarly low isotopic values (<2 Ra, *Martelli et al.,* 2004). A similar behavior is also shown by a few measurements of the nitrogen isotopic composition ($\delta^{15}N$= 2.3 ‰ vs. air), which reflect a mixture of sediments and upper mantle fluids (*Sano et al.,* 2001). A detectable contribution of non-atmospheric, deep nitrogen also results from the $N_2/^{36}Ar$ ratios (2.60 x 10^4 to 1.72 x 10^5), which are higher than in air ($N_2/^{36}Ar$ = 2.46 x 10^4). The isotopic data of CdM methane ($\delta^{13}C_{CH4}$ -46.2 to -51.5‰ vs. PDB; δD_{CH4} -184.7 to -202 ‰ vs. SMOW) (Fig. 9) are similar to those published by *Ciotoli et al*. (2013).

The offshore gas is contaminated by air (O_2 ~9 vol.%) and has high CH_4 and He contents (in the air-corrected composition 59 vol.% and 33 ppm, respectively), possibly due to preferential CO_2 dissolution into seawater, which also caused the drastic reduction of its pH (see section 3.2 and Fig. 8). The offshore gas has more negative $\delta^{13}C_{CH4}$ and δD_{CH4} and lower $^3He/^4He$ than CdM (-60.5‰ vs. PDB and -209.7‰ vs. SMOW, R/Ra= 0.14, respectively). Excluding an isotope fractionation of CH_4 and He, due their low solubility in water, these characteristics suggest a CH_4 origin of the offshore gas from microbial CO_2 reduction likely occurring in peat-rich deposits of the Tiber delta and a lower contribution of mantle He then at CdM. The $\delta^{13}C_{CO2}$ of the offshore and CdM gases (-1.7 to -1.2 ‰ vs. PDB) is similar to other CO_2-dominated gas manifestations of the area and interpreted by many authors as due to mantle/magma degassing and/or limestone thermometamorphism (see introduction). In contrast to *Ciotoli et al.,* (2013), who suggested that CdM methane has a dominant thermogenic component, we think that methane at CdM, as well as at Canale Vignole site, is the result of a mixing, in different proportions, between:

1) abiogenic methane released from geothermal and volcanic-hydrothermal reservoirs (*Tassi et al*., 2012) and similar to that discharged at Palidoro;
2) microbially produced methane similar to the offshore gas.

As a matter of fact, notwithstanding the $\delta^{13}C_{CH4}$ and δD_{CH4} values at CdM are in the range typical for thermogenic sources (from -50 to -30 ‰ vs. PDB and from -250 to -100 ‰ vs. SMOW respectively), one would expect $CH_4/(C_2H_6+C_3H_8)$ ratios lower than 100. However, ethane and propane are present only at ppm level (Table 2), thus leading to $CH_4/(C_2H_6+C_3H_8)$ ratios between 5495 and 8881 (3685 at Canale Vignole) and therefore a thermogenic origin can be excluded.

4.3. Temporal monitoring of CdM gas emission

The plot of Fig. 10 strengthens the hypothesis that the close gas emissions of CdM, Canale Vignole and the offshore might be the result of a two endmember mixing process between a CH_4-dominated gas (very similar to the offshore gas and characterized by a $\delta^{13}C_{CH4}$ = -62 ‰) and a CH_4-poor term characterized by heavier CH_4 ($\delta^{13}C_{CH4}$ >-30 ‰). We highlight that CdM gases collected in different days plot along that mixing line. Focusing simply of the CdM temporal monitoring (Fig. 11), some clear simultaneous chemical and isotopic variations (He/CH_4 ratio and $\delta^{13}C_{CH4}$) are recognizable. We propose that these temporal variations are due to a change in the mixing proportions between the two endmembers. To better constrain the characteristics of the endmembers, in Fig 12 the $\delta^{13}C_{CH4}$ is plotted against the He/CH_4 ratio and the $^3He/^4He$ ratio. The curves are forced through the data points and are the only ones that may simultaneously fit the data set. Such mixing process is therefore compatible with the two following gaseous endmembers:

i) a gas (E1 in Fig. 12) characterized by a radiogenic He ($^3He/^4He$ = 0.03 Ra) and biogenic CH_4 ($\delta^{13}C_{CH4}$= -62 ‰, following the constraints of Fig. 10) and He/CH_4 ~2E-5, very similar to the gas emitted offshore;
ii) a gas (E2 in Fig. 12) characterized by higher $^3He/^4He$ (~0.25 Ra), heavier CH_4 ($\delta^{13}C_{CH4}$ ~ - 25 ‰), and He/CH_4 =4E-4. This second endmember could have a lower $\delta^{13}C_{CH4}$ (between -45 and

-25‰), but we prefer to choose the ~ -25 ‰ value because it represents the most extreme term among a continuous distribution of $\delta^{13}C_{CH4}$ in the Tyrrhenian area (between –40 and -25 ‰, *Tassi et al.,* 2012).

It is noteworthy that the second endmember has He/CH_4 and $^3He/^4He$ ratios similar to the gas emitted in the Fiumicino area (IS in Fig. 2) during the blowout occurred in 2005 (He/CH_4= 1.5-2.6 E-4; $^3He/^4He$= 0.31 Ra, *Barberi et al.,* 2007). Unfortunately, the $\delta^{13}C_{CH4}$ was not analyzed in the 2005 gas emission. Also, we suggest that the second gas endmember is more similar to gases emitted from the Sabatini region than to those from the Albani Hills (Fig. 1), given that the latter has a He/CH_4 ratio incompatible with our proposed mixing process (Fig. 12).

The first endmember could be generated in a shallow environment rich of radiogenic He and biogenic CH_4, and therefore isolated from eventual addition of deeply-derived gases. The second one could be slightly deeper and/or better connected to deep horizons, therefore subjected to enrichment of gas with a deeper signature (i.e., higher $^3He/^4He$ and $\delta^{13}C_{CH4}$). We therefore suggest that in the Fiumicino area several pockets of pressurized gas, with different chemical and isotopic characteristics, exist at depth of some tens of meters (*Barberi et al.,* 2007, *Sella et al.,* 2014), and may mix each other. The drilling of the CdM boreholes caused the gas blowout of one of this pockets, fed by a mixing between two different gases.

The temporal monitoring of CdM gas composition (Fig. 11) demonstrates that between 24 September and 25 October 2013 the system was perturbed by an increase of the shallower crustal endmember that produced a decrease in the He/CH_4 ratio and the $\delta^{13}C_{CH4}$ (Fig. 11). The system then slowly returned to its pristine conditions, as displayed by the simultaneous increase of the He/CH_4 ratio and the $\delta^{13}C_{CH4}$. A new sampling of CdM was performed in September 2014 and showed ratios similar to August 2013, when the blowout started, confirming that the borehole is mostly fed by the same gas pocket resulting from a mixing between the two different gases above discussed.

5. Soil CO_2 diffuse degassing

On 26 August 2013, soon after the blowout onset, a first soil CO_2 flux survey was carried out around the CdM gas emission, with 114 measurement points over 2800 m^2, distributed on a regular grid with 5 m spacing. The background threshold of this first survey was established at 20 g m^{-2} d^{-1} (Fig. 3) and the resulting flux map showed that part of the gas rising from vent 1 was diffusing laterally within the sandy permeable soil. It was also clear that gas was preferentially diffusing towards NE in the direction of Fiumicino International Airport (Fig. 13). Around the vent, a target area for periodic monitoring of the soil CO_2 release was then established, with 94 fixed measurement points on a surface of 2354 m^2, extending from the roundabout toward the airport (Fig. 13). Unfortunately, some high emissive points nearest to the vent could not be measured in the subsequent surveys because they were rapidly covered by the emitted mud (see Figs. 04 and 05 in Supplementary Material). Nine new soil CO_2 flux surveys were carried out from 28 August to 29 September 2014, the latter nine months after cementation of the holes (Table 3). Some selected soil CO_2 flux maps are shown in Fig. 13; their related semivariograms are reported in Supplementary Material (Fig. 06). The mean and the maximum flux values increased with time up to 627 and 6425 g m^{-2} d^{-1} respectively (survey of 18 September), with a corresponding increase in the total diffuse CO_2 flux above the background threshold up to 1.8 ton/day (Table 3). From October, the soil CO_2 flux surveys were no longer representative of the total soil diffuse degassing because the most emissive area nearest to the gas emission could not be surveyed.

In order to investigate whether the gas diffusion from the boreholes was affecting also the inhabited zone nearby, on 13 September 2013 a wider survey was carried out outside the CdM target area, with 97 measurement points over a surface of 126,000 m^2. Only a few values exceeding the background threshold were found, mostly south of CdM (maximum= 104 g m^{-2} d^{-1}) but being not connected to the boreholes it was estimated that they did not represent a hazard. On 7 March 2014, nearly three months after the cementation of the boreholes, the soil CO_2 flux had strongly decreased, but some values above the background threshold (up to 144 g m^{-2} d^{-1}) persisted in the area between the vents and the airport (Fig. 13 and Table 3).

Six months later, on 29 September 2014, a new soil CO_2 flux survey found values similar to those measured before the borehole cementation (Table 3). The related soil CO_2 flux map (Fig. 13) clearly shows that gas was still being emitted from the boreholes and diffusing preferentially toward N, as in the previous surveys (Fig. 13). This implies that cementation failed to efficiently seal the CdM boreholes. Cementation aims to restore continuity in the impervious cover above the layer containing the pressurized gas, so preventing gas emission to the surface. In the 2005 Fiumicino gas blowout this was made by injecting cement into the boreholes obtaining a perfect result (*Barberi et al*., 2007). In the CdM 2013 operation, the boreholes were instead re-drilled and cased, and only the cased space was filled with cement, so leaving an uncemented portion around the case, through which gas continues to escape.

6. Simulation of CO_2 dispersion in the atmosphere and hazard assessment

The simulation of the CO_2 dispersion by Eulerian TWODEE-2 code (*Folch et al*., 2009) has been successfully applied to reproduce the CO_2 dispersion from natural sources over flat (*Costa et al*., 2008) and complex topography (*Chiodini et al*., 2010).

In our simulations, the topographic domain extended over an area of 1×1 km (Figs. 2 and 14a) which was discretized using a square grid with 200×200 cells with 5 m side. The area is almost flat (0.9 m to 3.0 m a.s.l.), gently sloping towards the sea (at northwest). The roughness of the soil changes from 0.001 to 0.02 m for bare or scarcely vegetated soils, tarmac areas and water surfaces, to 0.50-0.70 m for the inhabited area with only low to moderate height buildings. The CO_2 output was obtained by adding the viscous flux from the two vents (VF) to the diffuse soil flux (DF). Two days (18 and 24 September 2013) with a similar total CO_2 output were considered (17.44 and 19.82 ton day^{-1} respectively), but with different values of VF and DF (VF= 15.64 and DF= 1.8 ton/day on 18 September; VF= 19.12 and DF= 0.70 ton/day on 24 September). Wind data were recorded every hour by an automatic station (see location in Fig. 2 and Fig. 03 in Supplementary Material). On 18 September, the wind blew preferentially from the land (NNE to S) and subordinately from the sea

(W-WNW), whereas on 24 September the wind blew from the sea during the day (SW to W) and from the land during the night (NNE to E) (Fig. 14d e 14h). The condition recorded on 24 September is frequent over the Tyrrhenian coast of Italy because of the well-developed breeze regime controlled by thermally-induced sea-land air circulation (*Granieri et al.,* 2013).

The air CO_2 concentrations calculated at heights of 0.2, 1.0 and 1.5 m are shown in Fig. 14; they are expressed in vol.% as values in excess above the background air CO_2 concentration level (a.b.l.) which is 385 ppm, as measured in October 2013 far from the degassing area. As expected, the CO_2 plume is "anchored" to the gas source and preferentially follows the ground (Fig. 14), flowing towards the sea because of its negative buoyancy due to gravity control. The maximum CO_2 air concentrations are obviously found near the gas source, where the simulated mean value at 0.20 m was 3.4% on 18 September and 4.5% on 24 September. In a small area of a few hundred square meters around the vents (Fig. 14), the highest CO_2 concentrations occurred early in the morning (8.2% at 9:00 Local Time, LT) and during the night (7.9% at 23:00 LT) on 18 September and after dawn and during the night on 24 September (14.4% at 7:00 and at 23:00 LT). Near the gas source, lower concentrations, however never below 1.0%, characterized the central hours of both days. The day-night variations in air CO_2 concentration reflect efficient gas dispersion during the day by more intense wind circulation and gas accumulation during the night due to low or null winds (Fig. 14d and 14h). The gas plume rapidly diluted by moving away from the source region and mixing with "fresh" air at the edges of the cloud. Thus the CO_2 concentration decreased to <200 ppm a.b.l. on the lee side of the computational domain (about 0.5 km from the gas source, Figs. 14c and 14f). Similarly, the concentration of the CO_2 plume sharply decreased with elevation, conserving, in a very limited sector around the gas source, values up to ~1000 ppm at a height of 1.0 m (Fig. 14b and 14e) and up to ~500 ppm (Fig. 14a) and ~350 ppm (Fig. 14d) at a height of 1.5 m on 18 and 24 September respectively. Considering the whole area affected by the plume, the CO_2 increase was on average 240 ppm (a.b.l.), 30 ppm and 19 ppm at heights of 0.2 m, 1.0 m and 1.5 m on 18 September and 522 ppm, 38 ppm and 21 ppm at the same heights on 24 September.

Air CO_2 concentration was monitored, at a height of 0.8 m, by two continuous devises near the gas source and, at 0.3 m height, by the station monitoring also the environmental parameters located 10 m south from the gas vents (Fig. 2). At 0.8 m the maximum value (3.6 vol.%) was measured on 15 September (at 12:00 LT); on 18 and 24 September the maximum measured value was 1.33 vol.% (at 10:00 LT) and 0.9 vol.% (at 20:00 LT) respectively (Fig. 15A and 15B). At 0.3 m height the upper limit (5 vol.%) of the [CO_2] analyser was repeatedly reached (Fig. 15C).

Considering the limitations due to the Eulerian approach in reproducing the dispersion in the highly transient gas source region (*Boybeyi and Raman,* 1995), the agreement between measured and simulated values is acceptable. In addition, we must consider that small dead mammals were repeatedly found within 10-15 m of the vents; this implies that a lethal CO_2 concentration (>8 vol.%, *Carapezza et al*., 2011) was frequently reached here, in agreement with the simulation results.

7. Conclusions

The gas blowouts occurred in summer 2013 near Rome (Fiumicino International Airport, Italy) confirm that a large onshore and offshore part of this area, including densely populated zones (Fig. 2), contains pressurized gas pockets at a shallow depth (tens of meters) within the fluvial and lagoonal Tiber delta deposits. The distinctive feature of Fiumicino zone is a widespread rising along deep reaching faults of deep originated CO_2, which pressurizes the shallow aquifer largely fed by seawater in the coastal plane and confined underneath an impervious clay layer. Rising CO_2 may mix in these superficial layers with methane of microbial origin. The gas blowout occurs anytime the pressured aquifer is reached by a well.

An impressive amount of greenhouse gases was emitted into the atmosphere in nearly four months, up to ~20 ton day^{-1} of CO_2 and 99 kg day^{-1} of CH_4, for a total emission (viscous plus diffuse) of over 1500 tons of CO_2 and 5.4 tons of CH_4. Peaks of air CO_2 concentrations up to 14.4 vol.% were estimated during night or early morning at a height of 0.20 m near the CdM emission, where small dead animals were frequently found. An air CO_2 concentration of 3-4 vol.% was systematically found throughout the day, exceeding the *NIOSH* (1997) short time exposure limit (STEL= 3 vol.% for 15 minutes).

Fortunately, the most exposed area was inside a road roundabout, which was immediately fenced off, preventing people from entering it. The air CO_2 concentration rapidly decreased moving away from the source, so that the large inhabited sector near the emission and the airport area (Fig. 14) were only affected by a diluted gas cloud with concentrations not exceeding 1000 ppm (a.b.l.). Such concentrations exclude an immediate risk for humans but could sustain a build/up of CO_2 to dangerous concentrations in the basements of poorly ventilated houses or in morphological depressions in the soil (*Carapezza et al.,* 2011; *Granieri et al.,* 2013). At heights of 1.0 m and 1.5 m, which are the typical breathing heights for vehicle drivers and for standing humans, no dangerous CO_2 concentrations were found, though systematic alteration of pure air locally occurred, with CO_2 and CH_4 enrichment.

The frequency of gas blowouts in the region of Rome calls for rigorous gas hazard assessment, with particular attention to urban areas. Fiumicino appears to be a particularly risk prone area, including the International Airport of Rome and the sea just off it, where the occurrence in summer season of a gas blowout like that of September 2013 would create serious problems for sea traffic and swimmers.

The temporal monitoring of the onshore gas emission allowed to recognize a mixing of two CO_2-dominated gas sources, characterised by distinct chemical (He/CH_4 ratio) and isotopic ($^3He/^4He$, $\delta^{13}C_{CH4}$, δD_{CH4}) signatures. The first source is generated in a shallow environment, while the second is better connected to deep horizons and fed by gas with a deeper signature. The various soil gas flux surveys performed in different moments at CdM also highlighted that the cementation performed four months after the blowout failed to definitively seal the boreholes, in contrast to what happened during a previous gas blowout occurred in the area in 2005.

This study underlines that an accurate temporal monitoring of this kind of phenomena may help to increase our knowledge on the origin of gases, the existence of eventual multiple gas reservoirs and on the correct actions to be undertaken in order to restore the natural environmental equilibrium in presence of pressurized gas pockets. In turn, this is useful to better address the environmental gas hazard assessment in areas, such that of Fiumicino, particularly prone to this risk.

Acknowledgements. The cost of the onshore research was covered by a contribution of the Civil Protection Department of Regione Lazio to Fiumicino Municipality. The offshore research was financially supported by a contract to INGV of the Fiumicino Port Authority. Arnaldo De Benedetti and Guido Giordano of the University of Roma Tre–Science Department contributed to the field measurements of the viscous flux. Mariano Tantillo of INGV-Palermo contributed to the isotopic analyses.

References

Appelo, C.J., and D. Postma (1994), Geochemistry, Groundwater and Pollution, *Balkema, Rotterdam*, 2nd ed., pp. 519.

Barberi, F., M.L. Carapezza, M. Ranaldi, and L. Tarchini (2007), Gas blowout from shallow boreholes at Fiumicino (Rome): Induced hazard and evidence of deep CO_2 degassing on the Tyrrhenian margin of Central Italy, *J. Volcanol. Geotherm. Res., 165*, 17-31.

Bigi, S., S.E. Beaubien S.E., G. Ciotoli, C. D'Ambrogi, C. Doglioni, V. Ferrante, S. Lombardi, S. Milli, L. Orlando, L. Ruggiero, M.C. Tartarello, P. Sacco (2014), Mantle-derived CO_2 migration along active faults within an extensional basin margin (Fiumicino, Rome, Italy). *Tectonophysics*, *637*, 137-149.

Boybeyi, Z., and S. Raman (1995), Simulation of elevated long-range plume transport using a mesoscale meteorological model, *Atmos. Environ., 29*, 2099–2111.

Capelli, G., and R. Mazza (2008), Intrusione salina nel delta del Fiume Tevere. In: R. Funiciello, A. Praturlon, and G. Giordano (Eds.), Evoluzione del fenomeno nei primi anni del terzo millennio (in italian), *Mem. Descr. Carta Geol. d'Italia.* 80, 237-260.

Carapezza, M.L., and D. Granieri (2004), CO_2 soil flux at Vulcano (Italy): comparison between active and passive methods, *Appl. Geochem., 19*, 73-88.

Carapezza, M.L., and L. Tarchini (2007), Accidental gas emission from shallow pressurized aquifers at Alban Hills volcano (Rome, Italy): geochemical evidence of magmatic degassing?, *J. Volcanol. Geotherm. Res., 165*, 5-16.

Carapezza, M.L., Badalamenti, B., Cavarra, L., and A. Scalzo (2003). Gas hazard assessment in a densely inhabited area of Colli Albani Volcano (Cava dei Selci, Roma). *J. Volcanol. Geotherm. Res.* 123, 81–94.

Carapezza, M.L., F. Barberi, L. Tarchini, M. Ranaldi, and T. Ricci (2011), Volcanic hazard of the Colli Albani, In: R. Funiciello and G. Giordano (Eds.), The Colli Albani volcano, Spec. Publ. IAVCEI, *Geological Society, London*, 3, 279–297.

Carapezza, M.L., F. Barberi, M. Ranaldi, T. Ricci, L. Tarchini, J. Barrancos, C. Fischer, D. Granieri, C. Lucchetti, G. Melian, N. Perez, P. Tuccimei, A. Vogel, and K. Weber (2012), Hazardous gas emissions from the flanks of the quiescent Colli Albani volcano (Rome, Italy), *Appl. Geochem., 27*, 1767–1782.

Chiodini, G., Cioni, R., Guidi, M., Raco, B., Marini, L., 1998. Soil CO_2 flux measurements in volcanic and geothermal areas. *Appl. Geochem.* 13, 135–148.

Chiodini, G., C. Cardellini, A. Amato, E. Boschi, S. Caliro, and F. Frondini (2004), Carbon dioxide Earth degassing and seismogenesis in Central and Southern Italy, *Geophys. Res. Lett., 31*, doi: 10.1029/2004GL019480.

Chiodini G., D. Granieri, R. Avino, S. Caliro, A. Costa, C. Minopoli, and G. Vilardo (2010), Nonvolcanic CO_2 Earth degassing: Case of Mefite d'Ansanto (southern Apennines), Italy. *Geophys. Res. Lett.,, 37*, L11303, doi:10.1029/2010GL042858.

Costa, A., G., Chiodini, D., Granieri, A. Folch, R. Hankin, S. Caliro, R. Avino, and C. Cardellini, (2008), A shallow layer model for heavy gas dispersion from natural sources: application and hazard assessment at Caldara di Manziana, Italy. *Geochem. Geophys. Geosystems, 9*, Q03002, doi: 10.1029/2007GC001762.

Cinti, D., M. Procesi, F. Tassi, G. Montegrossi, A. Sciarra, O. Vaselli, and F. Quattrocchi (2011), Fluid geochemistry and geothermometry in the western sector of the Sabatini Volcanic District and the Tolfa Mountains (Central Italy), *Chem. Geol., 284*, 160-181.

Ciotoli, G., G. Etiope, F. Florindo, M. Marra, L. Ruggiero, and P.E. Sauer (2013), Sudden deep gas eruption nearby Rome's airport of Fiumicino, *Geophys. Res. Lett., 40,* doi:10.1002/2013gl058132.

Douglas, S., and R. Kessler (1990), In: Carr, L. (Ed.), User's Manual for the Diagnostic Wind Model, *San Rafael, CA*, III, EPA-450/4-90-007C.

Folch A., A. Costa, and R.K.S. Hankin (2009), TWODEE-2: A shallow layer model for dense gas dispersion on complex topography, *Comput. Geosci., 35*, 667-674, doi: 10.1016/j.cageo.2007.12.017.

Granieri D., A. Costa, G. Macedonio, M. Bisson, and G. Chiodini (2013), Carbon dioxide in the urban area of Naples: contribution and effects of the volcanic source, *J. Volcanol. Geotherm. Res., 260,* 52–61.

Grassa F., G. Capasso, Y. Oliveri, A. Sollami, P. Carreira, M.R. Carvalho, J.M. Marques and J.C. Nunes (2010), Nitrogen isotopes determination in natural gas: analytical method and first results on magmatic, hydrothermal and soil gas samples, *Isot. Environ. Health Stud.*, *46*, 141–155.

Martelli, M., P.M. Nuccio, F.M. Stuart, R. Burgess, R.M. Ellam, and F. Italiano (2004), Helium-strontium isotope constraints on mantle evolution beneath the Roman comagmatic province, Italy, *Earth Planet. Sci. Lett., 224,* 295-308.

McCrea J. (1950), On the isotopic chemistry of carbonates and a paleotemperature scale, *J. Chem. Phys*., *18,* 849-857.

Milli, S., C. D'Ambrogi, P. Bellotti, G. Calderoli, M.G. Carboni, A. Celant, L. DiBella, F. Di Rita, V. Frezza, D. Magri, R.M. Pichezzi, and V. Ricci (2013), The transition from wave-dominated estuary to wave-dominated delta: The Late Quaternary stratigraphic architecture of Tiber River deltaic succession (Italy), *Sedimentary Geol., 284-285*, 159-180.

Minissale, A., W.C. Evans, G. Magro, and O. Vaselli (1997), Multiple source components in gas manifestations from north-central Italy, *Chem. Geol., 142,* 175-192.

NIOSH (National Institute of Occupational Safety and Health) (1997), Pocket Guide to Chemical Hazard, *DHHS (NIOSH), 97-140, U.S. Gov. Print Office, Washington, DC.*

O'Nions, R. K., and E. R. Oxburgh (1988), Helium volatile fluxes and the development of continental crust, *Earth Planet. Sci. Lett., 90,* 331-347.

Paonita, A., A. Caracausi, G. Iacono-Marziano, M. Martelli, and A. Rizzo (2012), Geochemical evidence for mixing between fluids exsolved at different depths in the magmatic system of Mt Etna (Italy), *Geochim. Cosmochim. Acta*, *84*, 380-394

Raich, J.W., H. Lambers, and D.J. Oliver (2014), Respiration in terrestrial ecosystems, reference module in Earth systems and environmental sciences, in Treatise on Geochemistry (II Edition), *Elsevier, Amsterdam,* 10, 613-649.

Sano Y., N. Takahata, Y. Nishio, T.P. Fischer, and S.N. Williams (2001), Volcanic flux of Nitrogen from the Earth, *Chem. Geol*., *171*, 263-271.

Tassi F., J. Fiebig, O. Vaselli, and M. Nocentini (2012), Origin of methane discharging from volcanic-hydrothermal, geothermal and cold emissions in Italy, *Chem Geol*., *310-311*, 36-48.

Terzić, J., Z. Peh, and T. Marković (2010), Hydrochemical properties of transition zone between fresh groundwater and seawater in karst environment of the Adriatic island, Croatia, *Environ. Earth Sci., 59*, 1629-1642.

Trabelsi, R., K. Abid, K. Zouari, and H. Yahyaoui (2012), Groundwater salinization processes in shallow coastal aquifer of Djeffara plain of Medenine, Southeastern Tunisia, *Environ. Earth Sci., 66*, 641-653.

Figure captions

Figure 1. Main volcanic features and location of the natural gas emissions in the Thyrrenian side of Central Italy. The main faults of the zone between Fiumicino and Rome, buried and inferred from seismic profiles, are shown in the insert (after *Milli et al*., 2013).

Figure 2. Fiumicino area with location of 2013 onshore (CdM) and offshore (OS) gas blowouts, of natural gas emission (stars) and of other gas blowouts occurred in the same area (dots). Black square shows the area of numerical simulation of CO_2 dispersion in the atmosphere. The insert shows the road roundabout where the two onshore boreholes were located (vent 1 to SW), the CO_2 soil flux measurement points (small dots), the location of the gas air concentrations station (triangles) and the meteorological station (square). Pictures (from left) show the offshore gas emission, the CdM vent 1 degassing into atmosphere and during viscous gas flux measurement. IS: Isola Sacra, CV: Canale Vignole, PG: Ponte Galeria.

Figure 3. Normal probability plot of soil CO_2 flux measurements of 26 August 2013 survey. Anomalous flux of endogenous origin is characterized by values exceeding the background threshold, estimated at 20 g m^{-2} d^{-1}.

Figure 4. Time variation of viscous flux from boreholes: CO_2 (black circle) and CH_4 (grey diamond) from 30 August to 30 October 2013.

Figure 5. A 27 September 2014 picture of the offshore gas blowout (location in Fig. 1).

Figure 6. Seabottom section across the offshore gas vent as reconstructed by sonar surveys and sub inspections during (left) and after (right) the gas emission.

Figure 7**.** Profiles of T, pH and electrical conductivity measured in seawater on the offshore vent on 2 October 2013. Note that, from -3m, values are constant for all the parameters, indicating that the gas emission had ceased.

Figure 8. Seawater pH variation during and after the gas blowout. *Black arrow*: onset of the gas blowout; *grey arrow*: end of the gas emission.

Figure 9. Isotopic composition of hydrogen and carbon of methane of studied samples expressed in ‰ vs. SMOW for H and ‰ vs. PDB for C.

Figure 10. Methane concentration and carbon isotope composition of studied samples. The curve represents a possible mixing process able to fit the collected data. The CH_4-rich end-member is constrained at CH_4 close to 100% and $\delta^{13}C_{CH4}$ ~ -62‰. It is worth of note that the offshore sample (CH_4 concentration= 59%) might be enriched in CH_4 due to CO_2 dissolution into seawater (see text). Anyway, the shift toward originally-lower CH_4 concentration does not cause a variation in the curve shape down to CH_4 concentration close to 5%.

Figure 11. Temporal plot of He/CH_4 and $\delta^{13}C_{CH4}$ of CDM gases. The last sampling of 29 September 2014, is also plotted.

Figure 12. Panel a: He/CH_4 vs $\delta^{13}C_{CH4}$ plot. Panel b: $^3He/^4He$ vs $\delta^{13}C_{CH4}$. CdM samples and the nearest free gases of the area are shown. The curves are mixing lines forced through the data points and are the only ones that may simultaneously fit the data set. Such mixing process is used to constrain the possible end-members, named E1 and E2 (see text). The Palidoro sample, as well as the other gases of Albani Hills, cannot be considered part of the mixing process because of their high He/CH_4 ratio. Albani Hills and Mt. Sabatini fields after *Barberi et al*. (2007) and *Tassi et al*. (2012).

Figure 13. Maps of soil CO_2 flux from August 2013 to September 2014. Color scale, scale bar and vertex coordinates (datum: WGS84, 33T) refer to all maps. Full star: emitting borehole; Black circle: cemented borehole.

Figure 14. Average (24-h) maps of air CO_2 concentration (above the local background content) at 0.2, 1.0 and 1.5 m of height on 18 September (*a*-*c*) and on 24 September 2013 (*e*-*g*). White areas in

the centre of the domain of Figs. 14*a* and 14*e* delimit the zones where air CO_2 concentration is >3 vol. % (Fig. 14*a*) and >4 vol.% (Fig. 14*e*). Rose diagram of the wind direction is shown in *d)* and *h)* with the correspondent wind speed for each sector (in brackets); the “c” indicates “calm” for that direction (i.e., wind speed < 0.1 m/s).

Figure 15. Results of air CO_2 monitoring near the CdM vents in September 2013 (see Fig. 2 for location). A and B refer to the devices placed, at 0.8 m height from the soil, respectively near vent 2 and vent 1. C: data recorded, at 0.3 m height from the soil, at the station monitoring also environmental parameters. Concentration values are expressed in ppm above the background air CO_2 concentration (385 ppm).

Figure1

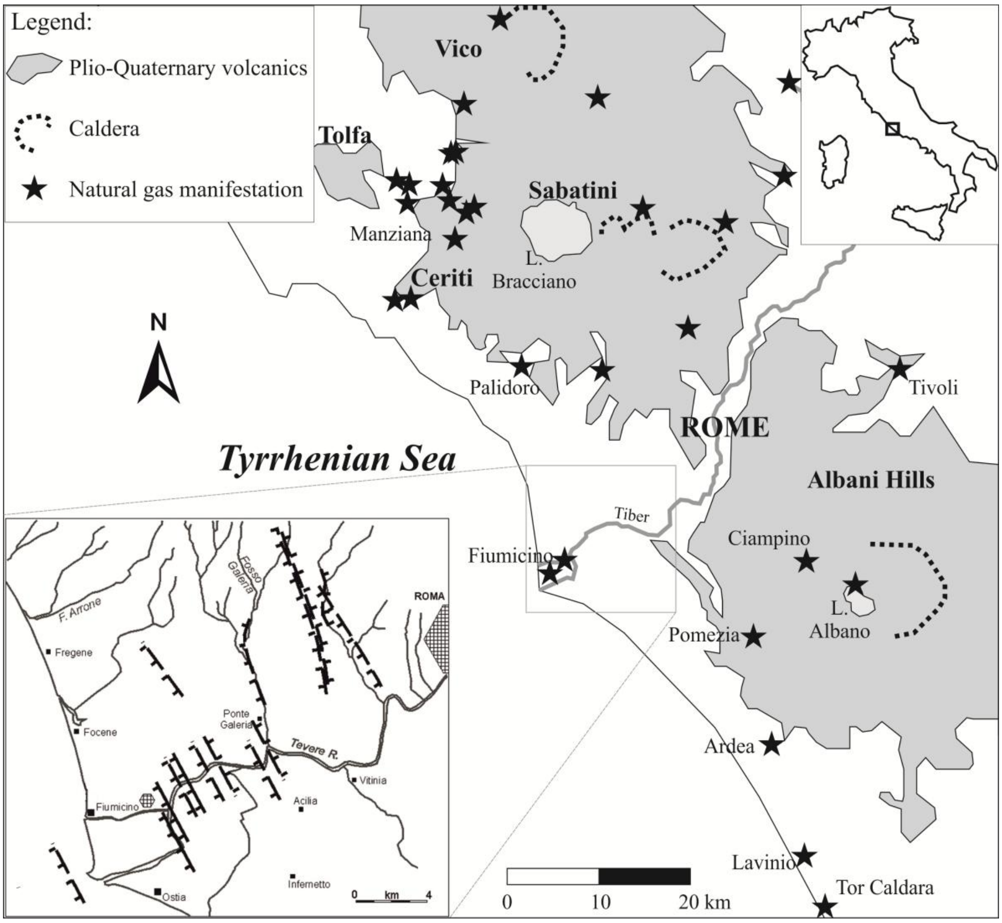

Fig. 1. Main volcanic features and location of the natural gas emissions in the Tyrrhenian side of Central Italy. The main faults of the zone between Fiumicino and Rome, buried and inferred from seismic profiles, are shown in the insert (after *Milli et al*., 2013).

Figure2

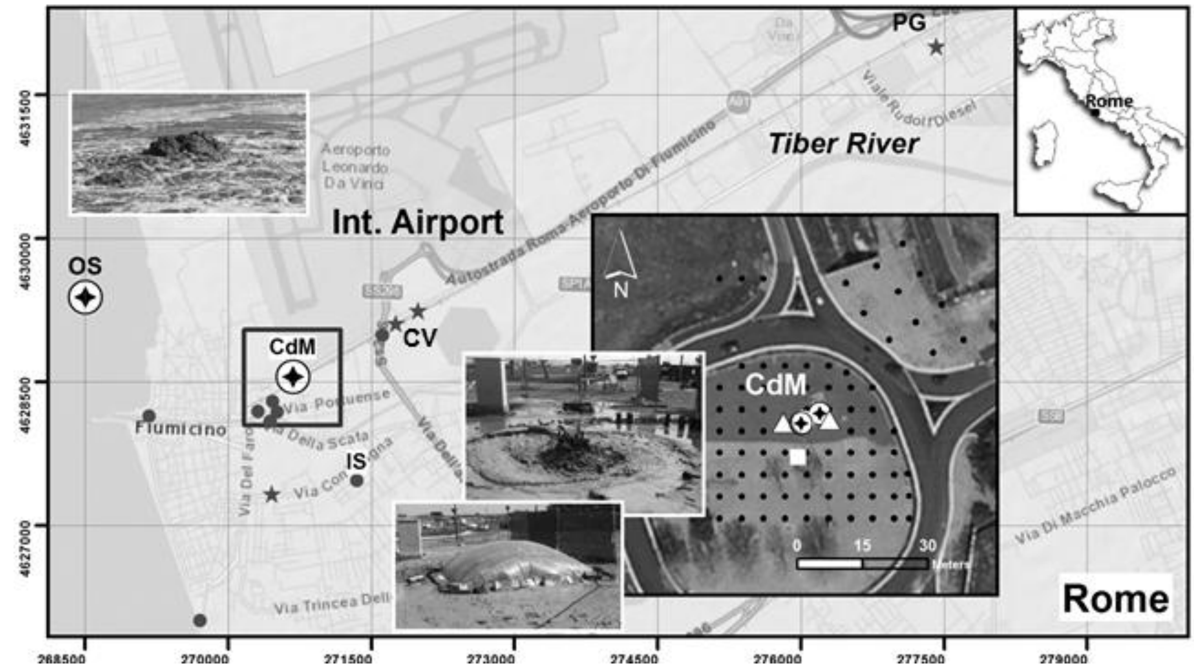

Fig. 2. Fiumicino area with location of 2013 onshore (CdM) and offshore (OS) gas blowouts, of natural gas emission (stars) and of other gas blowouts occurred in the same area (dots). Black square shows the area of numerical simulation of CO_2 dispersion in the atmosphere. The insert shows the road roundabout where the two onshore boreholes were located (vent 1 to SW), the CO_2 soil flux measurement points (small dots), the location of the gas air concentrations station (triangles) and the meteorological station (square). Pictures (from left) show the offshore gas emission, the CdM vent 1 degassing into atmosphere and during viscous gas flux measurement. IS: Isola Sacra, CV: Canale Vignole, PG: Ponte Galeria.

Figure 3

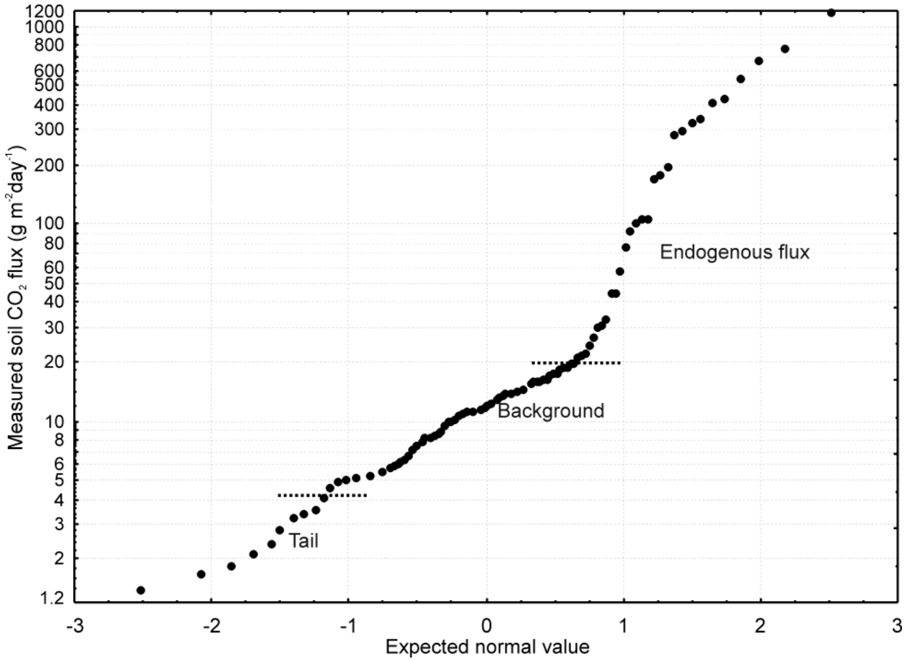

Fig. 3. Normal probability plot of soil CO_2 flux measurements of 26 August 2013 survey. Anomalous flux of endogenous origin is characterized by values exceeding the background threshold, estimated at 20 g m^{-2} d^{-1}.

Figure 4

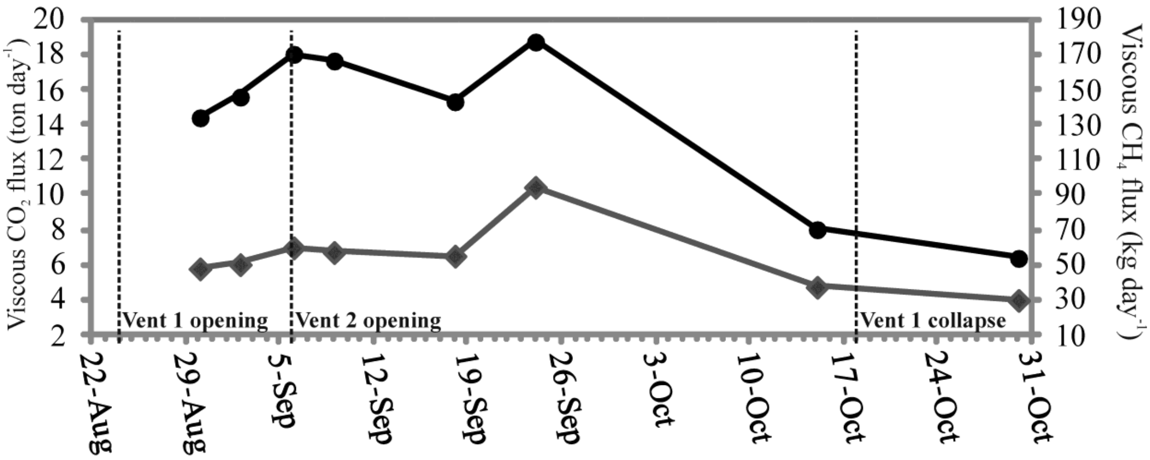

Fig. 4. Time variation of viscous flux from boreholes: CO_2 (black circle) and CH_4 (grey diamond) from 30 August to 30 October 2013.

Figure 5

Fig. 5. A 27 September 2014 picture of the offshore gas blowout (location in Fig. 1).

Figure 6

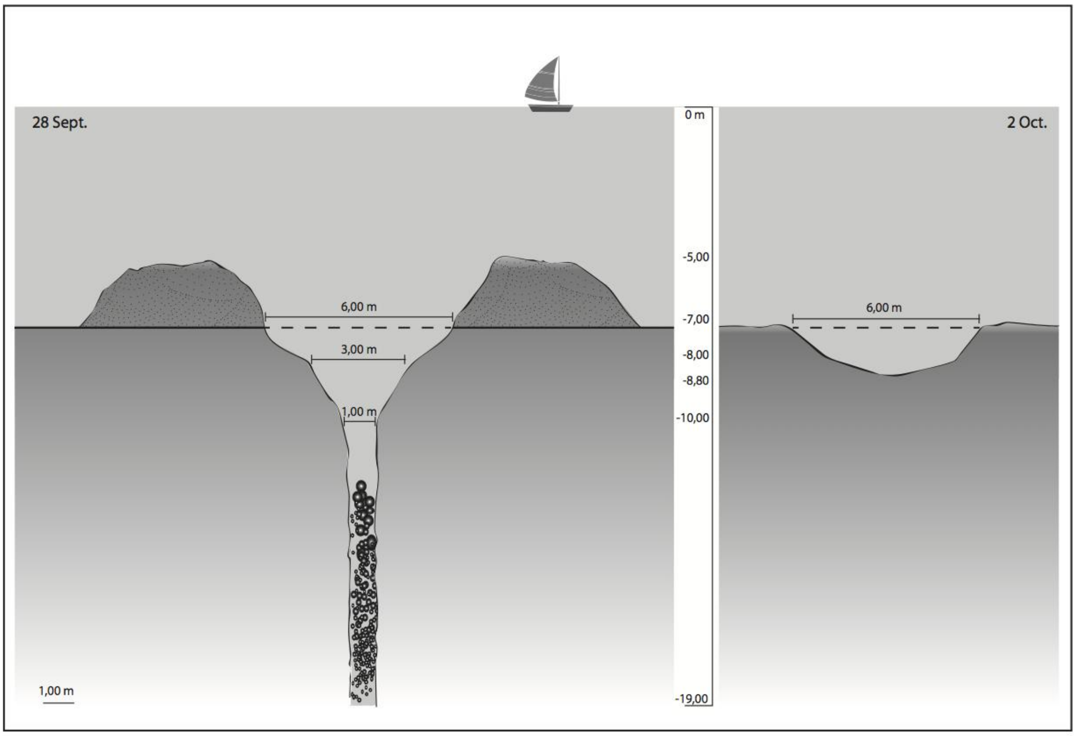

Fig. 6. Seabottom section across the offshore gas vent as reconstructed by sonar surveys and sub inspections during (*left*) and after (*right*) the gas emission.

Figure 7

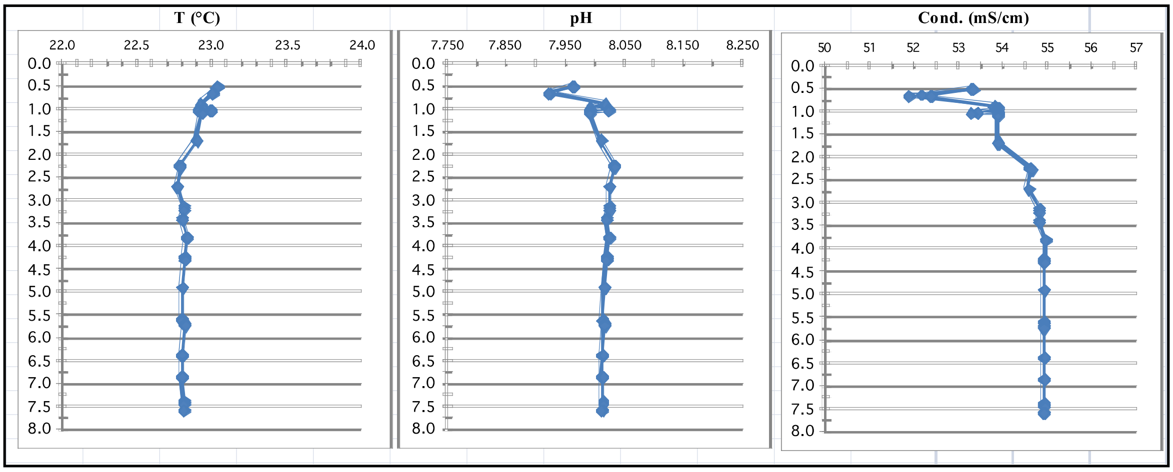

Fig. 7. Profiles of T, pH and electrical conductivity measured in seawater on the offshore vent on 2 October 2013. Note that, from -3m, values are constant for all the parameters, indicating that the gas emission had ceased.

Figure 8

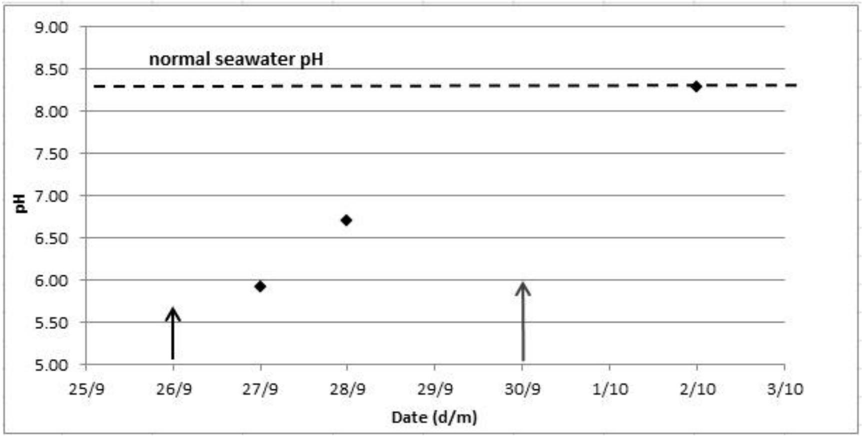

Fig. 8. Seawater pH variation during and after the gas blowout. *Black arrow*: onset of the gas blowout; *grey arrow*: end of the gas emission.

Figure 9

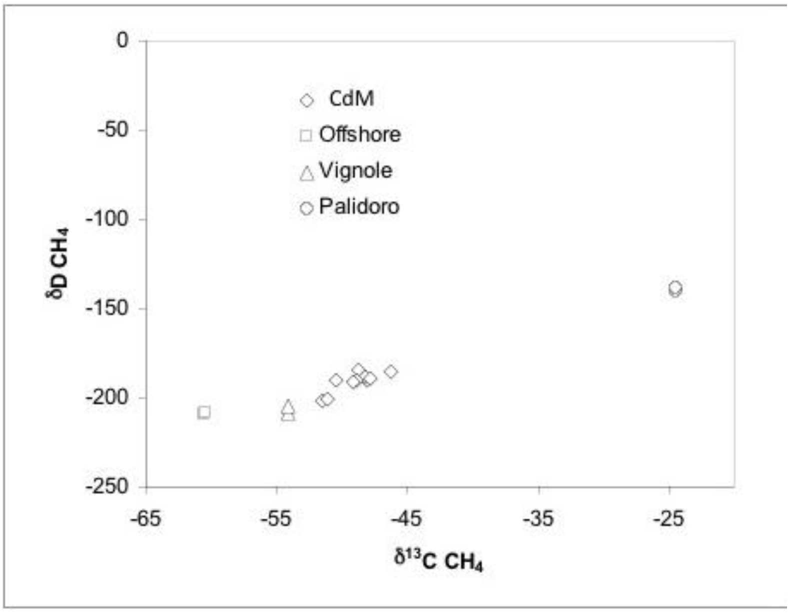

Fig. 9. Isotopic composition of hydrogen and carbon of methane of studied samples expressed in ‰ vs. SMOW for H and ‰ vs. PDB for C.

Figure 10

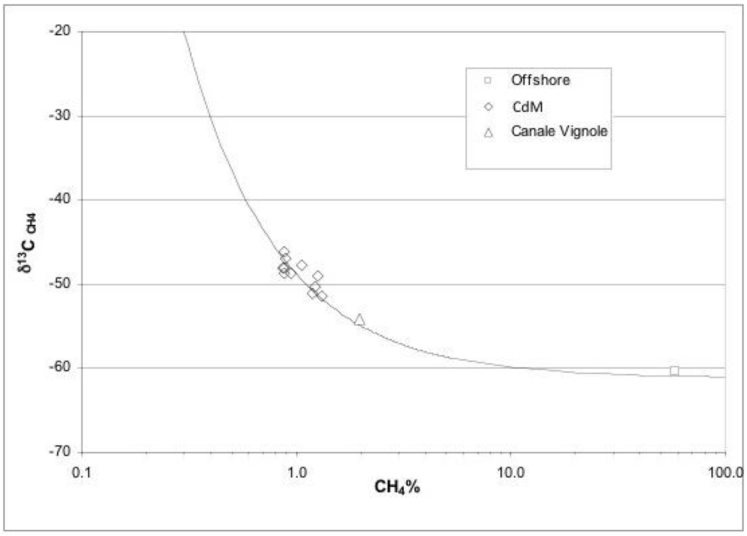

Fig. 10. Methane concentration and carbon isotope composition of studied samples. The curve represents a possible mixing process able to fit the collected data. The CH_4-rich end-member is constrained at CH_4 close to 100% and $\delta^{13}C_{CH4}$ ~ -62‰. It is worth of note that the offshore sample (CH_4 concentration= 59%) might be enriched in CH_4 due to CO_2 dissolution into seawater (see text). Anyway, the shift toward originally-lower CH_4 concentration does not cause a variation in the curve shape down to CH_4 concentration close to 5%.

Figure 11

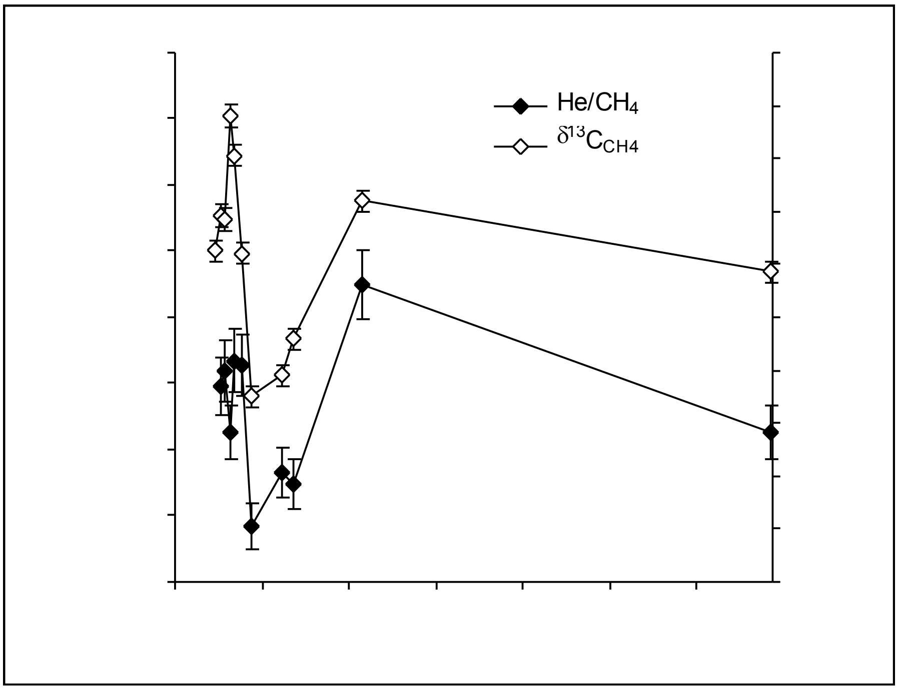

Fig. 11. Temporal plot of He/CH_4 and $\delta^{13}C_{CH4}$ of CDM gases. The last sampling of 29 September 2014, is also plotted.

Figure 12

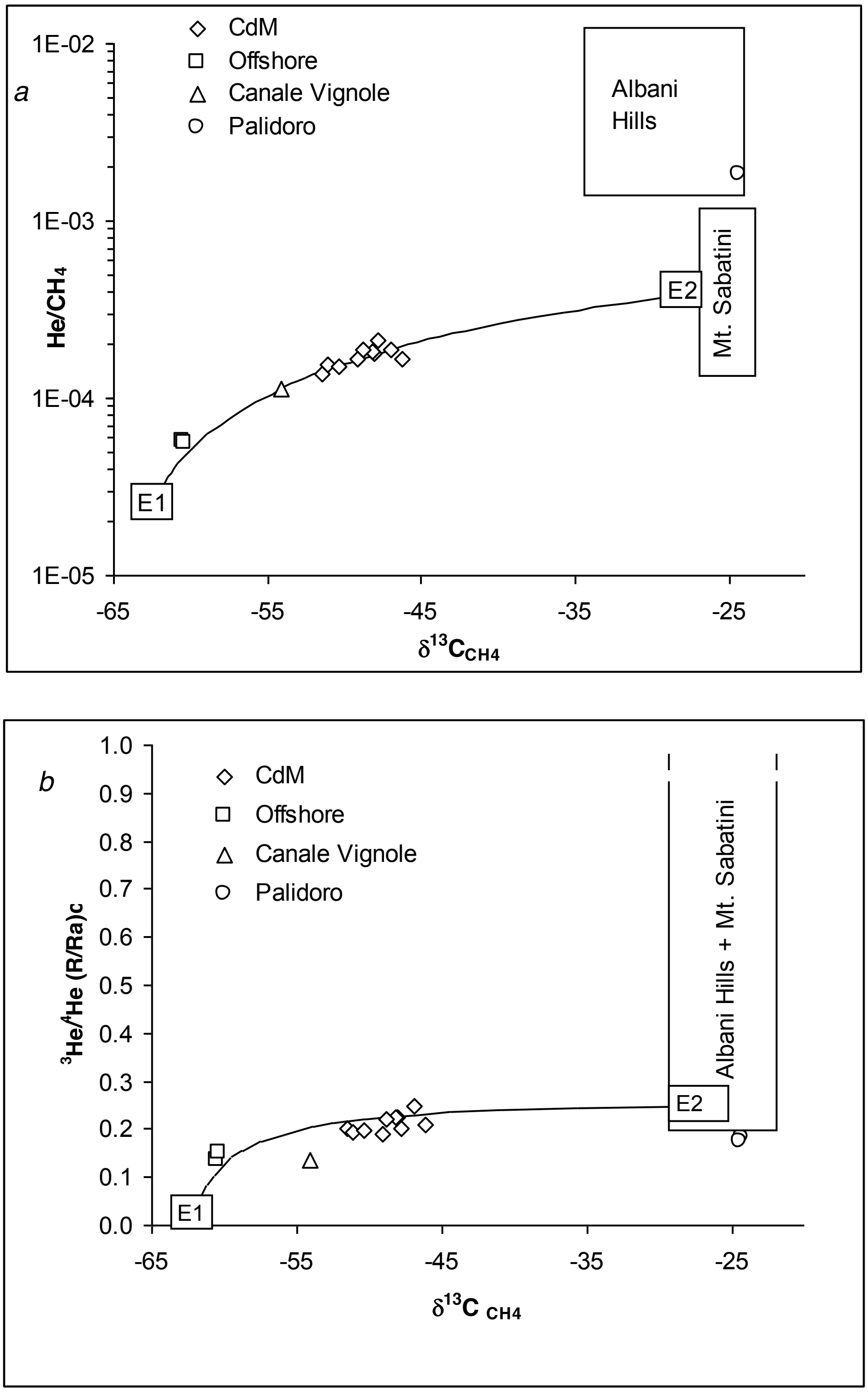

Fig. 12. *Panel a*: He/CH_4 vs $\delta^{13}C_{CH4}$ plot. *Panel b*: $^3He/^4He$ vs. $\delta^{13}C_{CH4}$. CdM samples and the nearest free gases of the area are shown. The curves are mixing lines forced through the data points and are the only ones that may simultaneously fit the data set. Such mixing process is used to constrain the possible end-members, named E1 and E2 (see text). The Palidoro sample, as well as the other gases of Albani Hills, cannot be considered part of the mixing process because of their high He/CH_4 ratio. Albani Hills and Mt. Sabatini fields after *Barberi et al*. (2007) and *Tassi et al*. (2012).

Figure 13

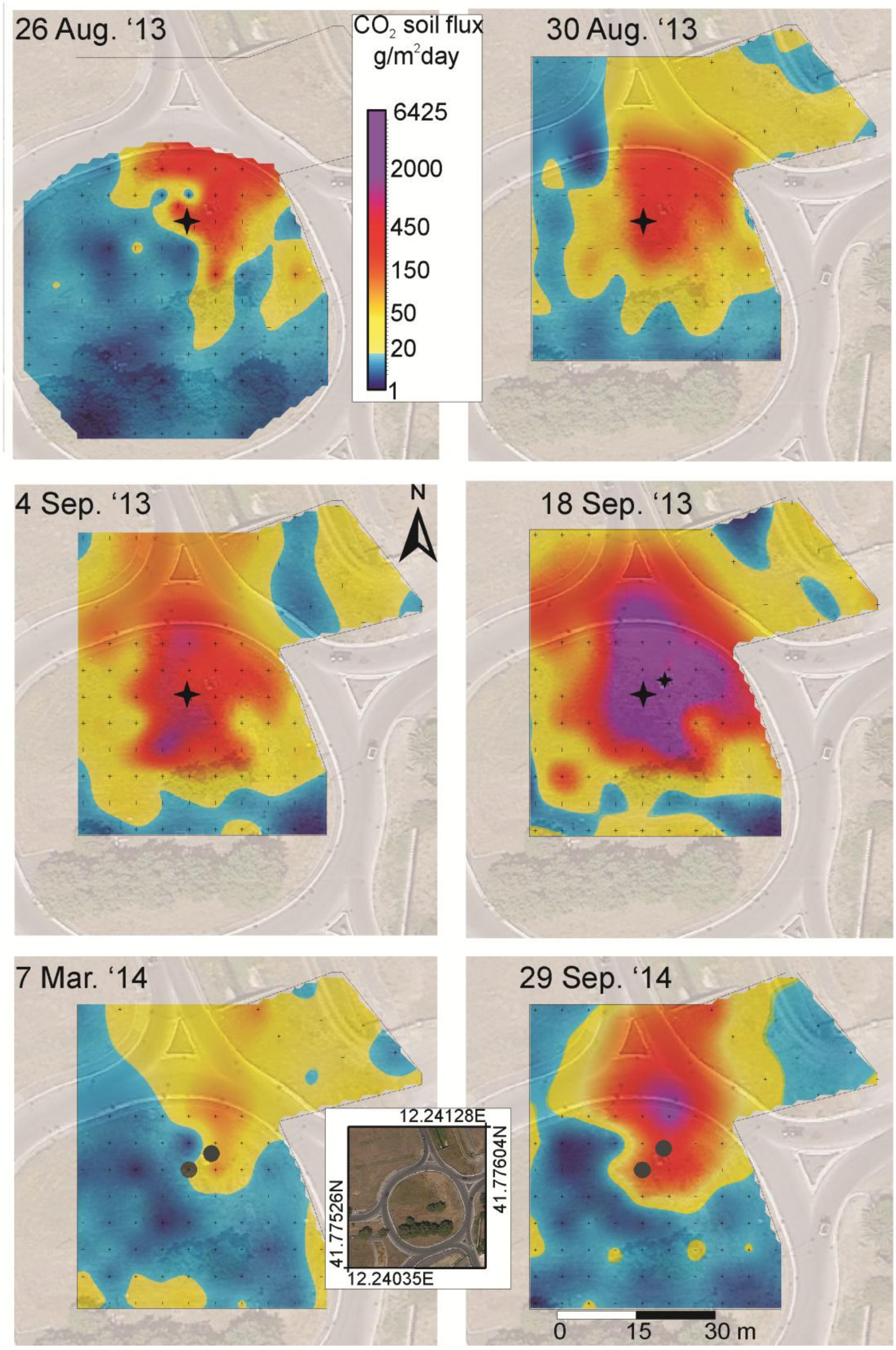

Fig. 13. Maps of soil CO_2 flux from August 2013 to September 2014. Color scale, scale bar and vertex coordinates (datum: WGS84, 33T) refer to all maps. *Full star*: emitting borehole; *Black circle*: cemented borehole.

Figure 14

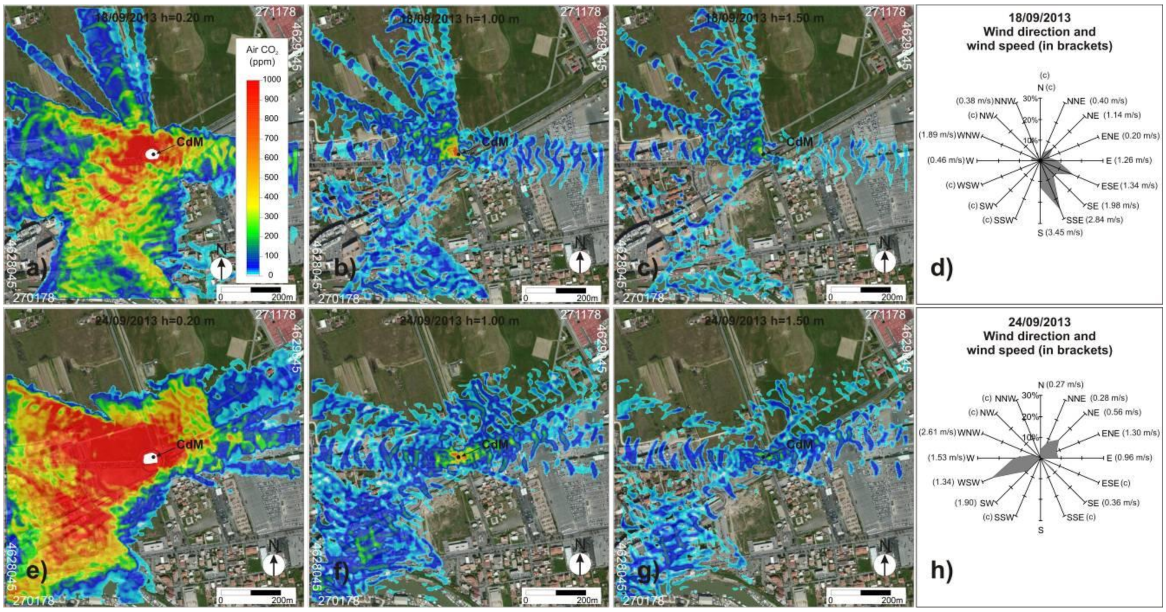

Fig. 14. Average (24-h) maps of air CO_2 concentration (above the local background content) at 0.2, 1.0 and 1.5 m of height on 18 September (*a*-*c*) and on 24 September 2013 (*e*-*g*). White areas in the centre of the domain of Figs. 14*a* and 14*e* delimit the zones where air CO_2 concentration is >3 vol. % (Fig. 14*a*) and >4 vol.% (Fig. 14*e*). Rose diagram of the wind direction is shown in *d)* and *h)* with the correspondent wind speed for each sector (in brackets); the "c" indicates "calm" for that direction (i.e., wind speed < 0.1 m/s).

Figure 15

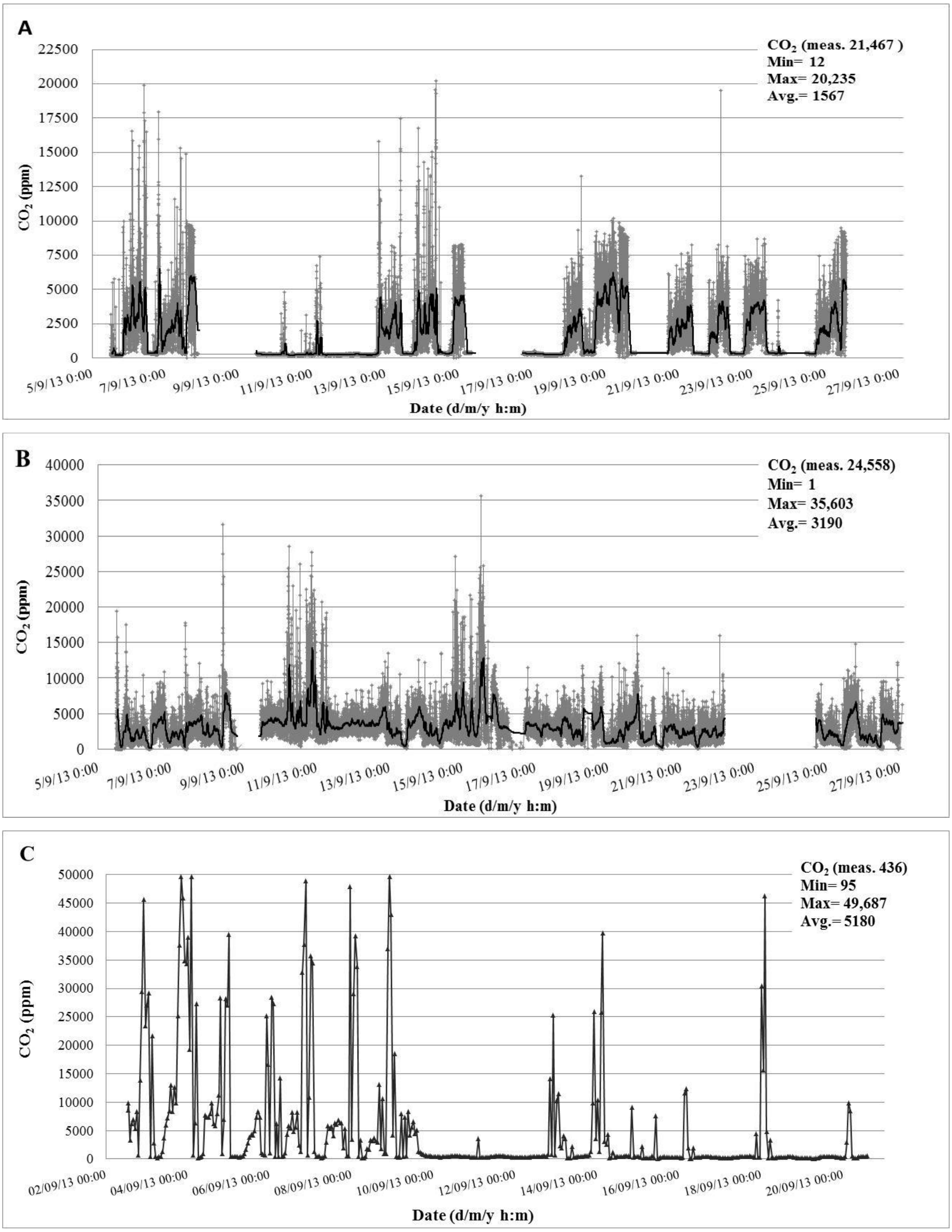

Fig. 15. Results of air CO_2 monitoring near the CdM vents in September 2013 (see Fig. 2 for location). A and B refer to the devices placed, at 0.8 m height from the soil, respectively near vent 2 and vent 1. C: data recorded, at 0.3 m height from the soil, at the station monitoring also environmental parameters. Concentration values are expressed in ppm above the background air CO_2 concentration (385 ppm).

Table 1-3

Table 1. Composition of the water emitted at CdM, vent 1 (September 2013)

Sample	T	pH	Eh	TDS	Cl^-	Br^-	NO_3^-	SO_4^{2-}	HCO_3^-	Na^+	K^+	Mg^{2+}	Ca^{2+}	$\delta^{13}C_{TDIC}$ (meas.)	$\delta^{13}C_{CO2}$ (calc.)	Seawater mixing ratio
#	°C		mV	g/L	mmol/L	mg/L	mg/L	mmol/L	mmol/L	mmol/L	mmol/L	mmol/L	mmol/L	‰ vs.PDB	‰ vs.PDB	
CdM	19.0	6.51	105	27.79	482.20	128.0	< 1	0.09	117.00	373.68	8.57	107.48	17.86	8.79	3.20	66 %

Table 2. Chemical and isotopic characteristics of sampled gases

Sample	date	He	Ar	O_2	N_2	CH_4	CO_2	C_2H_6	C_3H_8	$^4He/^{20}Ne$	$^4He/^3He$	$^{40}Ar/^{38}Ar$	$\delta^{13}C_{CH4}$	$\delta^{13}D_{CH4}$	$\delta^{13}C_{CO2}$	$\delta^{15}N_{N2}$
#	d/m/y	ppm	ppm	%	%	%	%	ppm	ppm		(R/Ra)c		‰ vs.PBD	‰ vs.SMOW	‰ vs.PBD	‰ vs. air
CdM	30/08/2013	n.m.	84	0.13	1.58	0.89	97.3	n.m.	n.m.	n.m.	n.m.	300.3	-48.7	-184.7	-1.4	n.m.
CdM	03/09/2013	1.6	52	0.08	1.40	0.87	98.1	1.2	0.2	26.2	0.22	302.6	-48.1	-190.0	-1.4	n.m.
CdM	05/09/2013	1.6	74	0.12	1.56	0.88	96.4	n.m.	n.m.	16.9	0.22	301.7	-48.2	-188.3	-1.4	n.m.
CdM	10/09/2013	1.5	37	0.04	1.27	0.88	98.2	1.4	0.2	54.2	0.21	306.8	-46.2	-185.3	-1.5	n.m.
CdM	12/09/2013	1.8	404	0.75	3.55	0.88	95.2	n.m.	n.m.	2.9	0.25	295.2	-47.0	n.m.	-1.4	n.m.
CdM	18/09/2013	1.8	111	0.20	1.89	0.95	96.0	n.m.	n.m.	9.4	0.22	294.0	-48.8	-190.5	-1.5	n.m.
CdM	24/09/2013	1.8	73	0.12	1.60	1.33	96.0	1.7	0.2	16.8	0.20	293.3	-51.5	-202.0	-1.5	n.m.
CdM	16/10/2013	1.8	32	0.05	1.38	1.19	96.4	1.2	0.1	32.5	0.20	296.2	-51.1	-200.5	-1.4	n.m.
CdM	25/10/2013	1.8	98	0.17	1.54	1.23	96.8	n.m.	n.m.	13.5	0.20	296.1	-50.4	-190.1	-1.2	2.27
CdM	12/12/2013	2.2	46	0.09	1.54	1.06	96.4	n.m.	n.m.	20.1	0.20	293.4	-47.8	-189.1	-1.4	n.m.
CdM	29/09/2014	2.1	n.m.	0.31	2.60	1.26	95.9	n.m.	n.m.	9.9	0.21	n.m.	-49.1	-191.7	n.m.	n.m.
***Offshore* 1**	27/09/2013	33.0	n.m.	0.09	18.3	59.3	22.3	n.m.	n.m.	3.0	0.13	n.m.	-60.5	-209.7	-1.7	n.m.
***Offshore* 2**	27/09/2013	32.0	n.m.	0.10	16.9	59.5	23.4	n.m.	n.m.	2.7	0.15	n.m.	-60.3	-208.7	-1.6	n.m.
Palidoro	18/10/2013	1.5	66	0.11	1.24	0.08	97.0	n.m.	n.m.	15.1	0.18	296.0	-24.4	-140.3	-1.8	n.m.
Palidoro	12/12/2013	1.5	47	0.08	1.10	0.08	97.3	n.m.	n.m.	11.3	0.17	326.8	-24.5	-138.7	-1.7	1.46
Can. Vignole	12/12/2013	2.3	60	0.11	1.94	1.99	95.6	5.0	0.4	28.7	0.13	297.4	-54.1	-205.0	-1.5	n.m.
Isola Sacra	01/02/2005	1.7	n.m.	0.02	1.56	0.80	98.4	n.m.	n.m	43.9	0.31	n.m.	n.m.	n.m.	-1.5	n.m

IS: Isola Sacra, from *Barberi et al.* (2007). The chemical composition of offshore gas is corrected for atmospheric contamination assuming that all O_2 except 0.1% (coherently with CdM measurements) is atmospheric. Helium isotopes are also corrected for atmospheric contamination.

Table 3. Results of soil CO_2 flux surveys in the target area of CdM

Date	Measurements	Soil CO_2 flux values			Soil CO_2 flux above background threshold	
Date	Measurements	min	avg	max	Total flux	Anomalous area
Before well sealing	*no*	*$g\ m^{-2}d^{-1}$*	*$g\ m^{-2}d^{-1}$*	*$g\ m^{-2}d^{-1}$*	*$ton\ day^{-1}$*	*m^2*
26 Aug 2013	114	1.4	65	1174	0.12	770
30 Aug 2013	94	2.8	68	704	0.18	1460
04 Sep 2013	81	4.3	160	2884	0.33	1841
06 Sep 2013	84	5.6	119	1529	0.40	1838
09 Sep 2013	79	2.8	235	3608	0.69	1348
18 Sep 2013	76	8.4	627	6425	1.80	1957
24 Sep 2013	71	7.0	208	2402	0.70	1906
15 Oct 2013	70	9.2	66	562	0.17	1796
After well sealing						
07 Mar 2014	81	1.8	24	144	0.06	1423
29 Sep 2014	82	2.0	88	2595	0.27	1352

Investigated area, on 26 August 2013= 2800 m^2; CdM target area= 94 points over 2354 m^2

Supplementary Interactive Plot Data (CSV)

Click here to download Supplementary Interactive Plot Data (CSV): Carapezza et al_Supplementary Material.pdf